DOE/ET-53088-371 IFSR #371

Enhanced Radiation Driven by a dc Electric Field

T. Tajima, A.O. Benz[2], *M. Thaker*[3], and *J.N. Leboeuf*[4]
Department of Physics and Institute for Fusion Studies
The University of Texas at Austin
Austin, Texas 78712

May 1989

[2] *Institute of Astronomy, ETH, CH-8092 Zurich, SWITZERLAND*
[3] *Department of Physics, University of California, Los Angeles, CA 90024*
[4] *Oak Ridge National Laboratory, Oak Ridge, TN 37831*

ENHANCED RADIATION DRIVEN BY A dc ELECTRIC FIELD

T. TAJIMA[1], A.O. BENZ[2], M. THAKER[3], AND J.N. LEBOEUF[4]

ABSTRACT

Direct radiation by runaway electrons under a constant (dc) electric field is investigated. In a one-and-two-halves dimensional relativistic electromagnetic code, an electron beam propagates along the external magnetic field parallel to the dc electric field and quickly decays into a runaway tail sustained by the dc electric field. Electrostatic and transverse waves are observed at various (fixed for each particular run) angles of wave propagation. Both plasma waves and electromagnetic radiation are strongly enhanced by the runaway tail. In the linear and early nonlinear beam stages the electromagnetic wave energy is slightly enhanced as the associated electrostatic component of the waves together with the dc electric field traps and detraps electrons. In the late nonlinear (runaway) stage and with sufficiently large observing angle, bursts of electromagnetic wave energy occur, accompanied by fast perpendicular spreading of the distribution function, and coincide with clamping of runaway electron momenta. The most intense electromagnetic energy arising from the Landau resonance is in an ordinary mode with frequency around the plasma frequency (the beam-plasma mode) with a narrow frequency width. The amount of energy in the electromagnetic components can exceed half the total wave energy. The mode could be radiative if it propagates toward a more tenuous plasma. The present mechanism of driven radiation can be extremely bright, while it is bursty as clumps of electrons come in and out of resonance with unstable radiative modes. These processes may be of astrophysical interest in cases of strong currents. As a possible application, we consider millisecond radio spikes associated with solar flares. In this situation the possibility of the present mechanism yielding the radiation temperature in excess of 10^{15} K is not out of the question.

key words: solar flares, driven radiation, beam-plasma instability, radio emission

[1]Department of Physics and Institute for Fusion Studies, The University of Texas at Austin, Austin, Texas 78712

[2]Institute of Astronomy, ETH, CH-8092 Zurich, Switzerland

[3]Department of Physics, University of California, Los Angeles, CA 90024

[4]Oak Ridge National Laboratory, Oak Ridge, TN 37831

I. INTRODUCTION

Intense superthermal radiation from plasmas is often observed in astrophysical settings, particularly from violent phenomena such as the magnetospheric substorms, solar flares, pulsars, and accretion disks. The Bremsstrahlung is a single particle phenomenon, as is the synchrotron radiation, they both have a characteristic power dependence as a function of frequency. When we encounter superthermal radiation from plasmas, however, we look for collective processes of radiation as a possible mechanism. They are generally more narrow-banded. We may discern three types of collective processes of radiation. The first is that based on the particle-wave interaction, while the second is that due to the wave-wave interaction (see, for example, Sagdeev and Galeev, 1969). The third is the process of mode conversion from nonradiative to radiative modes. (i) The first process can be linear interaction such as the beam-plasma instabilities (Mikhailovskii, 1974), although invariably these instabilities turn into nonlinear stages. (ii) The second process is nonlinear in nature, simplest of which is the so-called three-wave interaction. A beat wave interaction, i.e., an electromagnetic wave may be "scattered" ("induced scattering") by an electrostatic wave and turn into a third wave, another electromagnetic wave (see, for example, Tajima, 1985). Sometimes coupling of more than three waves is important. A process called parametric instability for three-wave coupling as well as four wave coupling has been investigated in detail (Nishikawa, 1968). The second process tends to give a broad and fuzzy energy and wavenumber spectra. (iii) The third process can be linear or nonlinear. The mode conversion of an electromagnetic wave into an electrostatic wave has been studied extensively in laboratory laser-plasma experiments (for example, Kruer, 1988), the inverse process of which can be of course very much possible (Melrose, 1980). A linear mode conversion of an acoustic wave into an Alfvén wave has been investigated recently (Steinolfson, *et al.*, 1989). This process may be important for the situation where intense electrostatic plasma

waves are excited, which can be mode converted in an underdense plasma into propagating electromagnetic waves.

It is the first process of the particle-wave interaction that we wish to investigate in detail in the present article. A beam of particles emersed in a magnetized plasma can become unstable against electromagnetic plasma instabilities, some of which can radiate. These are well-known processes (Mikhailovskii, 1974). The beam particles collectively interact and emit electromagnetic modes as well as electrostatic modes. As a result, the beam particles are slowed down by the particle-wave interaction, such as the trapping of particles (Sagdeev and Galeev, 1969; Bell, 1965). When this happens, the ability of the beam to radiate decreases and eventually vanishes due to the saturation of the instability. In the present paper we explore a novel process of driven emission of radiation through the particle-wave interaction through which the brightness and the amount of energy of radiation can far exceed that of the conventional beam-plasma instabilities. We also try to characterize this process of driven radiation. The driver can be either an electric field or gravitational acceleration.

Electric fields parallel to the magnetic field are expected in many astrophysical situations, such as reconnection, particle beams, rotating magnetospheres, pulsars, accretion disks, and many more. These electric fields sustain particle acceleration, and accelerated particles in turn emit radiation. Investigation of these physical processes is of particular concern in the present paper. In this problem the electric fields may be regarded nearly constant in time and space compared with scales of radiation of interest. We thus take the electric fields as dc fields in the present paper. Components of the electric fields present in a plasma cause a variety of different phenomena, depending on their being parallel or perpendicular to the ambient magnetic field. The electric field component perpendicular to the magnetic field causes the $\mathbf{E} \times \mathbf{B}$ drift motion of the plasma and the physics of this has been studied by many authors, including Schmidt (1960) and Koga *et al.* (1989). In the present article we focus on the case where the dc electric field is parallel to the ambient field if any.

Among a variety of possible phenomena, runaway particle acceleration as well as intensified coupling between plasma waves (electrostatic and/or electromagnetic) and particles are of interest in particular. These processes have already been noted in laboratory plasmas some time ago. The dc electric field preferentially increases higher energy electrons, the higher the energy is, the smaller the collision frequency becomes. This is the basis for the formation of runaway electrons. Runaway electrons and their accompanied emission were observed in toroidal devices (Oomens, *et al.*, 1976) and anomalous drags or resistivities were reported in experiments (Hirose and Skarsgaard, 1976) and simulations (e.g., Boris, *et al.*, 1970). A substantial increase in the radiation yield has been observed for a traveling wave tube when a dc voltage is applied (Tammaru, 1981). Leboeuf and Tajima (1979a) have simulated the beam plasma interaction in presence of a dc electric field with only electrostatic interactions allowed. Their studies show that the runaway electrons act as convertors of dc electric energy into electrostatic ac wave energy. In turn, the enhanced plasma waves strongly retard the increase in runaway momentum by the dc field.

We report here on fully relativistic simulations for the magnetized cold beam-plasma interaction in presence of a dc electric field. In order to single out the relevant physics, we constrain the propagation of radiation to only one direction with respect to the dc electric field (or beam) direction. In general, of course, the radiation is emitted in various directions with respect to the dc electric field direction. When the wavevector of radiation is constrained only to the beam propagation direction and the guide field, the beam-plasma interaction is found to be purely electrostatic (as long as the ions are immobile) and the results of Leboeuf and Tajima (1979a) are recovered. At propagation angles θ different from zero, however, some coupling between beam and electromagnetic waves exists. It leads to radiation enhancement as well as an increase of electrostatic plasma wave energy, the former more pronounced over the latter as θ is increased. A runaway induced propagating mode appears in the transverse branch of the plasma dispersion relation with a phase and group velocity about

equal to the speed of light. The excitation of this mode is accompanied by increased drag on the runaway electrons and their clamping in momentum, a phenomenon observed also experimentally (Menyuk, *et al.*, 1977).

The new radiation mechanism may explain narrow-band bursty emissions connected to processes involving strong electric fields. As a possible application we consider a particular type of radio emission, called millisecond spikes, of recent interest in solar microwaves and decimeter wavelengths. Thousands of millisecond spikes can sometimes be observed during the phase of primary energy release of solar flares (review by Benz, 1986). They originate from extremely intense sources with brightness temperatures in excess of 10^{15}K. The investigation of spikes has spurred great interest in efficient radiation mechanisms. Coherent cyclotron emission (maser) has been proposed by Holman, *et al.* (1980) and explored by many other authors. Previously, Wu and Lee (1979; 1985) proposed the maser process for the auroral kilometric radiation (Gurnett, 1981) and then later also for the flare emission. They studied theoretically the mechanism of emission via the coherent cyclotron maser effect in the presence of the loss cone due to the converging (geo-)magnetic fields, as particles precipitated. Wagner, *et al.* (1983; 1984) studied this by electromagnetic computer simulation. Their observed spectra of waves corresponded closely with those of the AKR. On the other hand, this mechanism is an instability and thus their result did not show impulsive radiation characteristic. The radiation power grows exponentially as the instability sets in and saturates due to the quasilinear flattening of the velocity space distribution of electrons. The observed spike duration of only a few milliseconds in flare emission, however, is difficult to reconcile with the build-up time of a suitable velocity distribution. The exploration of alternative direct radiation processes is, at least, very desirable.

The organization of this paper is as follows. The simulation model is briefly described in Sec. II and its results presented in Sec. III. The wave spectra of the simulation are discussed and interpreted in Sec. IV. We devote Sec. V to applications in astrophysics, in particular

to a possible model for solar millisecond spikes observed at radio frequencies.

II. THE MODEL

The simulation model is a one and two-halves-dimensional (one space and three velocity and field dimensions) electromagnetic finite-size particle code (see for example, Tajima, 1989). The only direction of spatial variation is the x-direction which is also the direction of propagation of the waves. The magnetized beam-plasma systems consists of a Maxwellian bulk of electrons, complemented by bulk Maxwellian ions when they are mobile, and a cold relativistic electron beam. The system length is $256\lambda_{\mathrm{De}}$, where λ_{De} is the Debye length of the electrons at $\omega_{pe}t = 0$. The typical number of beam electrons and bulk electrons is 256 and 2304, respectively, so that the beam to background density ratio is $n_b/n_p = 1/9$. The speed of light is set at $c = 9v_{te}$, where v_{te} is the initial thermal velocity of the electrons and the initial beam electrons momentum is $p_b = 7.63mv_{te}$ where m is the electron mass. This yields a relativistic factor for the beam electrons $\gamma = 1.31$ at $\omega_{pe}t = 0$. When there is a dc field, it is applied to particles with momentum larger than the cut-off momentum $p_l = 6.0mv_{te}$. This is to model the energy dependent runaway phenomenon. The strength of the dc field is set equal to $\tilde{E}_{\mathrm{dc}} \left(= eE_{\mathrm{dc}}/m\omega_{pe}^2\Delta\right) = 0.2$, where ω_{pe} is the plasma frequency, e the charge of one electron, and Δ the unit grid spacing that is taken equal to the initial electronic Debye length. This dc field is below the collective threshold dc field E_c at which a pure runaway beam is obtained, $\tilde{E}_c = 1.25$ for $n_b/n_p = 0.11$ (Leboeuf and Tajima, 1979b), but above the Dreicer field (1957). When the ions are set to be mobile, the ion-to-electron mass ratio is $M_i/m_e = 10$ and the ion-to-electron temperature ratio is $T_i/T_e = 1$. Otherwise, $M_i/m_e = \infty$.

The constant magnetic field, along which the beam propagates and the dc field is applied, is for most cases of strength such that the electron cyclotron frequency $\omega_{ce} = \omega_{pe}$. This static magnetic field is tilted in the x-y-plane at various angles θ with respect to the x-axis. This

allows for quasi two-dimensional effects because we can effectively have two projections of the wavevector, one along the field and one perpendicular to it as illustrated in Fig. 1. However, mode-mode coupling effects between different angles are neglected in this model. Recall, however, that all field vectors as well as momenta (and velocities) of particle can point any direction in space spun by x, y, z-axes because of $1 - \frac{2}{2} D$ dimensionality of the code.

III. WAVE ENERGY ENHANCEMENT BY THE PRESENCE OF A dc ELECTRIC FIELD

The temporal evolution of plasma waves and radiation energy under the influence of a dc electric field is considered with various tilt angles of the magnetic field, dc electric field and beam propagation directions (all coinciding) with respect to the wavevector lying along the x-axis. The results without the dc field will be discussed first before going on to the more complex cases with the dc field. The words longitudinal and transverse refer to the directions with respect to the chosen wavenumber, while the words parallel and perpendicular are used to indicate the directions with respect to the ambient magnetic field direction. The word electrostatic field is also used for the longitudinal field.

a) Beam-plasma interaction without dc field

Figure 2 summarizes the beam-plasma interaction without dc electric field imposed in a plasma. Figure 2(a) is a plot of the maximum amplitude growth rate as a function of the tilt angle θ. Here the wavenumber is defined as $k = 2\pi m/L_x$ with L_x the total system length and m an integer. The theoretical growth rates obtained from a numerical solution of the electrostatic dispersion relation with beam of Godfrey, *et al.* (1975) [their Eq. (14)] are also displayed for reference. The electrostatic field energy is $E_x^2/4\pi$, which can be expressed in a sum of many k-modes as done in Fig. 2(d). The electrostatic growth rate approximately decreases with angle θ as

$$\gamma_g(\theta) \sim \gamma_g(0) \cos^2 \theta, \tag{1}$$

where $\gamma_g(0)$ is the growth rate for $\theta = 0°$.

We have plotted in Fig. 2(b) the maximally growing mode number in the electrostatic field (circles) and the magnetic field (triangles) as a function of tilt angle θ. In the electrostatic approximation, for simplicity, the dispersion relation of the plasma without beam can be written (Mikhailovskii, 1974) as

$$\omega^2 = \frac{1}{2}\left(\omega_{pe}^2 + \omega_{ce}^2\right) \pm \frac{1}{2}\left[\left(\omega_{pe}^2 + \omega_{ce}^2\right)^2 - 4\omega_{pe}^2\omega_{ce}^2\cos^2\theta\right]^{1/2}. \tag{2}$$

The upper root with the plus sign is referred to as ω_1 and the lower one as ω_2 hereafter. Their electromagnetic counterpart can also be identified as an upper hybrid-type branch for the former and a whistler-type branch for the latter. For $\theta \lesssim 45°$, the coupling is between the beam mode with frequency $\omega \simeq kv_b\cos\theta$ and the upper hybrid branch with asymptotic frequency $\omega \simeq \omega_1$. For $\theta > 45°$, the coupling occurs between the beam mode again with frequency $\omega \approx kv_b\cos\theta$ and the whistler branch with asymptotic frequency $\omega \approx \omega_2$. According to linear theory the wavevector of the excited mode is approximately given by

$$k_{1\alpha} \sim \frac{\omega_1}{v_b}\cos\theta, \qquad \theta \lesssim 45°, \tag{3}$$

$$k_{2\alpha} \sim \frac{\omega_2}{v_b}\cos\theta, \qquad \theta > 45°. \tag{4}$$

These linear theory estimates agree with the simulation results.

The simulations show that saturation of the beam-plasma instability happens by merging of the beam with the background plasma or enhanced Landau damping (Dawson and Shanny, 1968; Kainer *et al.*, 1972). The plot of saturation times versus angle θ in Fig. 2(c) shows only a slight increase of the saturation time t_s up to $\theta = 45°$. Figure 2(d) is a plot of the saturation energies of the various field components normalized to the initial plasma kinetic energy with beam $n\kappa T_e$, as a function of tilt angle θ. For $\theta = 0°$, only the electrostatic

energy grows while the electromagnetic energies remain at the thermal level ($10^{-3}n\kappa T_e$). As the tilt angle is increased, the transverse magnetic energy overtakes the electrostatic energy.

b. Beam-plasma interaction with dc field

In the presence of the dc electric field (here $E_{\rm dc}$ is fixed at $0.2m\omega_{pe}^2\Delta/e$) a major difference is that after saturation of the initial beam-plasma instability (we will refer to this stage as the beam-plasma phase), the wave energy experiences a secular growth, attaining levels much higher than those achieved during the beam-plasma phase. The process of wave energy enhancement for $\theta > 0°$ is displayed in Fig. 3(a) the time evolution of all three components of the field energy as a function of time for the tilt angle $\theta = 15°$ with $\tilde{E}_{\rm dc} = 0.2$, and in Fig. 3(b) the same evolution but without dc field. The typical electrostatic field $E_{\rm es}$ at saturation with $E_{\rm dc} = 0$ may be estimated by $\frac{eE_{\rm es}}{m\omega_p v_b} \sim O(1)$, where v_b is the beam velocity. For relativistic beams, a more accurate expression reads (Thode and Sudan, 1973)

$$\frac{E_{\rm es}^2}{4\pi} = n_b\, mc^2\gamma_0 s_0(1+s_0)^{-5/2}\ , \tag{5}$$

where $s_0 = \gamma_0(n_b/2n_p)^{1/3}$ and $\gamma_0 = (1+p_0^2/m^2c^2)^{1/2}$. Equation (5) agrees well with Fig. 3(b). As can be seen from Fig. 3(a), the level of the electrostatic waves are enhanced approximately by a factor of three in terms of amplitude and the electromagnetic waves roughly by a factor of four over that of $E_{\rm dc} = 0$. We label this later energy increase as the runaway phase. The amplitude of the electromagnetic waves is about half the electrostatic waves just after the beam phase and about equal in the late phase of Fig. 2(a) for the $\tilde{E}_{\rm dc} = 0.2$ case. This means that the level of $E_{\rm es}$ is about one order of magnitude higher than $E_{\rm dc}$ and $E_{\rm em}$ is about half of $E_{\rm es}$ even in the early runaway phase. We will concentrate on the tilt angles $\theta = 15°$, $45°$, and $75°$; results identical to our electrostatic simulations (Leboeuf and Tajima, 1979a) are recovered here with $\theta = 0°$, unaffected by the presence of the guide magnetic field, since electromagnetic and electrostatic branches are decoupled and the beam only interacts with the electrostatic waves.

Take our example of $\theta = 15°$ for discussion. The beam-plasma phase ($\omega_{pe}\, t < 50$) has similar signatures with and without dc field. The beam energy is transferred preferentially to the electrostatic and magnetic fields. The modes with the highest energy in the beam-plasma phase for $\tilde{E}_{\rm dc} = 0.2$ are mode 5 for the longitudinal field and mode 6 for the transverse fields. The excited modes correspond to a coupling of the beam mode accelerated by the dc field, with its momentum evaluated at saturation as $p_s = p_b + qE_{\rm dc}t_s$ so that its velocity at saturation $v_s \simeq 7.51 v_{te}$, with frequency $\omega \simeq k v_s \cos\theta \sim \omega_{pe}$ and the upper hybrid-type branch at the same frequency. After saturation of the beam-plasma instability for $E_{\rm dc} = 0$, the energies rapidly subsided to a level somewhat over the thermal level as seen in Fig. 3(b). Conversion of beam energy to electromagnetic wave energy has stopped. This sharp decrease of the energies also takes place for $\tilde{E}_{\rm dc} = 0.2$. But all components of the field energy quickly start increasing again and by $\omega_{pe}t = 150$ have reached levels in excess of the beam-plasma phase ones where they remain for the rest of the run (up to $\omega_{pe}t = 400$) similar to the electrostatic runs (Leboeuf and Tajima, 1979a). Note that around $\omega_{pe}\, t = 400$ the energy content in the electromagnetic fields match or exceed that in the electrostatic fields. This is a salient feature of the present driven radiation process. It seems that the high level ES field saturates the process, while the EM waves do not directly contribute to the flattening of the electron distribution function.

The physical picture of the interaction is the following. The dc field accelerates particles with momentum greater than p_l, i.e., it creates runaway electrons. The fast electrons may be trapped by the waves giving up their kinetic energy to the wave potential energy. The trapped electrons under the dc electric field, however, receive acceleration. If the dc field acceleration surpasses the negative acceleration encountered by the electrons when they climb up the potential hill, the electrons will be detrapped. If the dc field acceleration is negligible compared with the acceleration (or deceleration) due to the wave, the electrons and the waves merely exchange energy. When the dc field acceleration is roughly matched

by the deceleration, due to the wave, of the electrons climbing up the potential barrier, the work done by the dc field is maximum, the condition for which is qualitatively given by Eq. (5): $E_{es} = E_{dc}$. The work done by E_{dc} is not necessarily funneled into an energy gain for the electrons but can be converted directly into wave energy (if the electrons do not climb up the potential hill) because of the phase-lock. The schematic phase space trajectories of Fig. 4 illustrate the above physical picture. The trapped electrons act as convertors of dc field energy into wave energy. This accounts for the rapid increase of electrostatic energy, illustrated in Fig. 3(a), after saturation of the initial beam-plasma instability by merging.

We summarize in Fig. 5 the behavior of the wave energy as a function of the tilt angle θ. We plot in Fig. 5(a) the maximum energies achieved by the longitudinal or electrostatic component of the electric field in the beam-plasma phase for $\tilde{E}_{dc} = 0$ (circles), in the beam-plasma phase for $\tilde{E}_{dc} = 0.2$ (dots), and in the runaway phase for $\tilde{E}_{dc} = 0.2$ (triangles). This procedure is repeated for the magnetic field and the transverse electric field. The maximum energies achieved in the interaction as a function of angle θ are plotted in Fig. 5(d): the electrostatic field is represented by circles and the magnetic field by triangles.

From Fig. 5(a), the trend of the electrostatic energy to decrease as a function of angle is repeated in all three phases. It decreases approximately as $\cos^2\theta$. The trend of the magnetic energy is to increase as a function of θ in both the beam-plasma phase with dc field and runaway phase. [cf. Fig. 5(b)] The ratio of magnetic energies in the beam-plasma phase with and without dc field is ~ 1.5 for $\theta = 15°$ and $\theta = 30°$ and more like a factor of 4 for $\theta = 45°$. The runaway phase energy is higher by a factor of 3 than the beam-plasma phase with $\tilde{E}_{dc} = 0.2$. For $\theta = 45°$, the magnetic energy in the runaway phase with $\tilde{E}_{dc} = 0.2$ is then enhanced twelve times over the same energy in the beam-plasma phase with $E_{dc} = 0$. This is further evidence of the strong interaction of the dc field driven runaways with the magnetic modes. Figure 5(c) also indicates a trend of the transverse electric energies in the beam-plasma phase and runaway phase for $E_{dc} = 0$ to increase as a function of angle.

The enhancement factor of the transverse electric energies between beam-plasma phase with and without dc field and of the runaway phase over the beam-plasma phase with dc field are equivalent to those achieved in the magnetic energies, but with lower energies achieved overall as compared to the magnetic energies. From Fig. 5(d) where the maximum wave energy is plotted as a function of tilt angle θ, the electrostatic energy usually dominates over the magnetic energy.

IV. WAVE SPECTRA

In the previous section we discussed the properties of beam-plasma interaction under the influence of $E_{\rm dc}$ in a spatially unresolved (global) analysis. In the present section we study the spatially resolved picture of the present interaction, i.e., we Fourier analyze the wave spectrum. A number of modes gain energy from runaway electrons. The wave spectrum is enriched by the presence of the guide magnetic field and its associated cyclotron branches. The dc field, which causes an increase of the momenta of the runaway electrons, leads to different, usually faster modes, being excited as time goes on. Constant trapping and detrapping of the runaway electrons under the combined influence of the waves and the dc field also leads to highly non-Maxwellian distribution functions with long runaway tails. The simulation dispersion relation may be obtained by the standard method (see, for example, Tajima, 1989).

a) Wave spectra for $E_{\rm dc} = 0$

The dispersion relation of both electrostatic and electromagnetic components are obtained in our simulations from temporal correlations of the corresponding fields. We compare these results to linear theory predictions.

The simulation dispersion relations is first compared with a numerical solution of the full electromagnetic dispersion relation without beam (Godfrey *et al.*, 1975) yielding the normal modes of the system, upon which we superimpose the beam mode at $\omega = kv_b \cos\theta$ and the

beam cyclotron resonances at $\omega_{\substack{\alpha \\ \beta}} = kv_b \cos\theta \pm \omega_{ce}/\gamma$ (if the need arises). We refer to this dispersion relation as the normal modes dispersion relation. This is a good method when the beam density is small. This first type of comparison is carried out for both electrostatic and electromagnetic modes. As a second approximation, we also compare the electrostatic simulation points with a numerical solution of the electrostatic dispersion relation with beam given by Godfrey *et al.* (1975) [their Eq. (14)]. We refer to this dispersion relation as the beam dispersion relation. This is justifiable because in many cases the electrostatic interaction is strong. An even simpler picture is provided by considering electrostatic normal modes and beam and beam-cyclotron resonances and picking out the cross-sections. This is illustrated in the figure in the book by Mikhailovskii (1974). Beam-cyclotron resonances are obtained from the cross-sections with the innermost oblique beam mode at $(\omega_2, k_{2\beta})$ and $(\omega_1, k_{1\beta})$. Cross-sections $(\omega_2, k_{2\alpha})$ and $(\omega_1, k_{1\alpha})$ are the beam mode resonances.

In terms of the polarizations of the normal modes in the full electromagnetic dispersion relation, the right-circularly polarized (R) and left-circularly polarized (L) modes are primarily defined from the parallel propagation characteristics of the waves, while the ordinary (O) and extraordinary (X) modes are primarily defined from their perpendicular propagation characteristics. However, for a case with a general tilt angle θ ($0 < \theta < 90°$), as is of interest here, modes may be defined in both ways. The cut-off frequencies, for the R waves and the L waves, are

$$\omega_{\pm}^{c} = \frac{1}{2}\left[\left(\omega_{ce}^2 + 4\omega_{pe}^2\right)^{1/2} \pm \omega_{ce}\right], \tag{6}$$

where ω_{+}^{c} is the R wave cut-off and ω_{-}^{c} is the L wave cut-off. The typical simplified dispersion relations for these modes are

$$c^2 k_{\parallel}^2/\omega^2 = 1 - \frac{\left(\omega_{pe}^2/\omega_{ce}^2\right)}{(1 \pm \omega_{ce}/\omega)}. \tag{7}$$

On the other hand, the frequencies of the O wave and the X wave may be characterized by

the ω_1 and ω_2 frequencies of Eq. (2), respectively. In the limit of $\theta \to \pi/2$, ω_1 tends to the upper hybrid frequency $\omega_h = \left(\omega_{pe}^2 + \omega_{ce}^2\right)^{1/2}$ and ω_2 tends to the lower hybrid frequency if ion effects are included (right now no ion terms are included and $\omega_2 \to 0$ as $\theta \to \pi/2$). The typical dispersion relations for the perpendicular O and X waves are, respectively,

$$\frac{c^2 k_\perp^2}{\omega^2} = 1 - \frac{\omega_{pe}^2}{\omega_{ce}^2}, \tag{8}$$

$$\frac{c^2 k_\perp^2}{\omega^2} = 1 - \left[\left(\frac{\omega_{pe}^2}{\omega^2}\right)\frac{\left(\omega^2 - \omega_{pe}^2\right)}{\left(\omega^2 - \omega_h^2\right)}\right]. \tag{9}$$

For an arbitrary tilt angle θ, modes with a smaller wavenumber are more easily classified as an R or L wave. As we come back to explain Fig. 6 later, in Fig. 6(c) for instance, at $k \to 0$, the highest frequency is the R wave cut-off frequency ω_+^c, the second one is ω_{pe} and the third one is ω_-^c. In the lower half of the ω-plane the order is reversed. At $k \to \infty$, the upper two branches (X and O modes in that order) tend to $\omega = kc$, the next one to ω_1, and the last one to ω_2. Similarly in the lower half of the ω-plane the order is reversed. For intermediate values of k, modes contain both features (R or L and X or O). A whistler-like mode may be seen in the lower branches of Fig. 6(c) between $1 \leq M \leq 6$. As θ increases the characteristics of the waves can be less identifiable as an R or L wave and more as an O or X wave.

We will see that there is good agreement between theory and the simulations. Cases for tilt angles $\theta = 15°$ and $\theta = 45°$ will be discussed in detail in this section. For $E_{\rm dc} = 0$, because of decoupling of the electrostatic and electromagnetic branches, the case for $\theta = 0°$ yields the usual electrostatic beam-plasma dispersion relation; the electromagnetic branch is only composed of the normal modes for a thermal plasma. We will therefore discuss the case $\theta = 0°$ only for $\widetilde{E}_{\rm dc} = 0.2$.

The electrostatic and electromagnetic dispersion relations for $E_{\rm dc} = 0$ and $\theta = 15°$ are plotted in Figs. 6(a), 6(b), and 6(c). In Fig. 6(a), the electrostatic peak frequencies are

compared to the theoretical normal mode dispersion relation; it is compared to the theoretical beam dispersion relation in Fig. 6(b). Note that the frequency spectrum is computed using the entire length of the time series of simulation. The electromagnetic dispersion relation of the simulation is compared to the theoretical normal modes in Fig. 6(c). This order of presentation will be followed thereafter. With regard to the theoretical normal mode dispersion relation and the theoretical electrostatic beam-plasma dispersion relation, we note that the cyclotron branches at $\omega = \omega_1$ and $\omega = \omega_2$, independent of the wavevector in the beam-plasma dispersion relation, are the asymptotes which the upper-hybrid and whistler branches (with frequencies dependent on the wavevector) tend to. At the short wavelengths or large mode and wave numbers and for small angles, these branches are degenerate in the beam-plasma dispersion relation.

Figures 6(a) and 6(b) show a clearly defined beam branch with $\omega = kv_b \cos\theta$ up to $M = 8$. This mode number corresponds to the cut-off in the growth rate from the theoretical beam dispersion relation. Branches at $\omega \simeq \pm\omega_{pe} = \pm\omega_{ce}$ which fall on the upper-hybrid branches of the electromagnetic normal modes are also present. Mode 7 has the highest spectral intensity and a frequency $\omega = (0.933 \pm 0.15)\omega_{pe}$ and coincides with the coupling of the beam branch at $\omega = kv_b \cos\theta$ and the upper-hybrid branch in the normal modes or degenerate cyclotron branches in the beam dispersion relation with frequency $\omega \sim \omega_{pe} = \omega_{ce}$. This most intense mode is on the branch of O-mode. Extraordinary branches are less intense. The maximally growing mode or the mode that achieves the highest energy in the beam-plasma phase in the electrostatic field E_x, i.e., from Sec. III, mode 8, has a frequency $\omega = (1.04 \pm 0.15)\omega_{pe}$ and is also the result of the same coupling. Note the remarkable sharpness of this mode. Its spectral width could not be well determined, since the plasma parameters (in particular the electron mass) change during the measurement and the applied data analysis broadens the peak. The simulations suggest a width far below 10% of the frequency. The magnetic modes are predominantly excited in the electromagnetic component of the spectrum of Fig. 6(c). The

spectral intensities achieved there are two orders of magnitude lower than their electrostatic counterparts. The beam branch is barely distinguishable in Fig. 6(c), a further indication of the weak coupling between beam and magnetic modes, already evidenced in Fig. 3(a), for a small tilt angle. Only mode 7 which has the highest spectral intensity might correspond to a beam mode. Mode 6 has, however, as high a spectral intensity in B_z and its frequency is determined to be $\omega = (0.63 \pm 0.2)\omega_{pe}$. This mode is observed only when the beam is slowed down. It is also the fastest growing mode. It intersects with the whistler branch. [The downshifting of the frequency towards the normal mode frequency is because the energy of this mode is sustained at a high level for only about $20\omega_{pe}^{-1}$ as compared to the correlation time of $100\omega_{pe}^{-1}$.] Mode 8 which also achieved a high energy in the magnetic modes has a measured frequency of $\omega = (0.875 \pm 0.25)\omega_{pe}$. The normal modes of the system are overall prominent in the electromagnetic branch of the spectrum and the whistler, upper-hybrid and light branches are well defined.

Without dc field, the beam therefore can directly couple to the upper hybrid-type branch with $\omega \sim \omega_{pe}$ and also to the whistler branch for large enough tilt angles. The effects of the coupling between the beam cyclotron modes and the normal modes of the system were too weak to be detected.

Figures 7(a), (b), and (c) correspond to the case with tilt angle $\theta = 45°$. The distinction between primarily electrostatic or electromagnetic modes is not easy since some whistler and light frequencies are imaged in the longitudinal field (E_x) simulation dispersion relations of Figs. 7(a) and (b). The beam branch is well defined there for $2 \leq M \leq 5$ and again for $9 \leq M \leq 14$. These two regions correspond for the first to the coupling of the beam branch with frequency $\omega \sim kv_b \cos\theta$ and the whistler branch or low frequency cyclotron branch which asymptotes to $\omega \sim \omega_2$. The second represents the coupling of the beam mode with the high frequency cyclotron branch or upper-hybrid branch with $\omega \sim \omega_1 \sim \omega_{pe} = \omega_{ce}$. Mode 4 has the highest spectral intensity of the modes in the first coupling region and its frequency

is $\omega = (0.3 \pm 0.10)\omega_{pe}$. Mode 11, which achieved the highest energy and is the most intense of the modes with $9 \leq M \leq 14$ has a frequency $\omega \simeq (1.0 \pm 0.15)\omega_{pe}$. It has the highest spectral intensity of the electrostatic modes. These two coupling regions also appear in the electromagnetic component of the wave spectrum of Fig. 7(c). The magnetic modes (B_z) have the highest spectral intensity. Mode 4 has the highest spectral intensity and the same frequency as measured in the electrostatic component, as does mode 11. Mode 9, which achieved the highest energy in the magnetic modes, has a frequency $\omega \simeq (0.84 \pm 0.10)\omega_{pe}$ and corresponds to a coupling of the beam with the upper-hybrid branch with $\omega \sim \omega_{pe}$.

b) Dispersion relations for $\tilde{E}_{\rm dc} = 0.2$

We now discuss cases with the dc field. We discuss here dispersion relations obtained from simulations with $\theta = 0°$, $\theta = 15°$, and $\theta = 45°$. We will compare the electrostatic and electromagnetic frequencies to the normal modes dispersion relation with the faster and denser beam mode with frequency $\omega = kv_f \cos\theta$ and the beam cyclotron modes with frequency $\omega = kv_f \cos\theta \pm \omega_{ce}/\gamma_f$ superimposed on it, where v_f and γ_f are determined from the time averaged runaway momentum p_f. The electrostatic simulation dispersion data will also be compared with a numerical solution of the electrostatic dispersion relation of Godfrey *et al.* (1975) with a faster (v_f) and denser ($\langle n \rangle$) beam. We will refer to this theoretical dispersion relation as the faster beam dispersion relation.

For $\theta = 0°$, the beam only interacts with the electrostatic modes with or without dc field. Therefore, we only compare here the electrostatic simulation dispersion relation with the faster beam dispersion relation. The simulation frequencies (dots) agree well with the faster beam dispersion relation (solid lines) as shown in Fig. 8. The modes with the highest spectral intensity lie on the faster beam branch with frequency $\omega \sim kc$. Note the coupling of the faster beam branch or runaway branch at $\omega \sim kc$ with the harmonics of the plasma branch at $\omega \sim 2\omega_{pe}$ and the start of one near $\omega \sim 3\omega_{pe}$. These harmonic branches are

not detectable without dc field. This dispersion relation except for the EM wave branch agrees with the one previously obtained in our purely electrostatic simulations (Leboeuf and Tajima, 1979a). Mode 6 is the most strongly excited in the runaway phase. This mode has the highest spectral intensity overall.

Figure 9 displays the simulation dispersion relations with dc field for the tilt angle $\theta = 45°$. The electrostatic simulation data plotted against the normal modes dispersion relation of Fig. 9(a) exhibits ω_1 and ω_2 branches and only partly the light branches. The modes with the highest spectral intensity lie on the faster beam branch or runaway branch with frequency $\omega \sim kv_f \cos\theta$ and $v_f \simeq 8.21 v_{te}$. The interesting feature in Figs. 9(a) and 9(b) is the presence (though weak) of the two cyclotron resonances at $\omega = kv_f \cos\theta \pm \omega_{ce}/\gamma_f$. With dc field, the distribution function has a long flat runaway tail which can support the high phase velocity mode $\omega = kv_f \cos\theta \pm \omega_{ce}/\gamma_f$. Similarly, the flatness or gentle sloping down of the tail may be the reason preventing the damping of the lower phase velocity mode with $\omega = kv_f \cos\theta - \omega_{ce}/\gamma_f$. Usually the latter mode is heavily damped since it falls close to the bulk of the plasma. Of all the modes on the runaway branch, mode 6 has the highest spectral intensity in the electrostatic component of the spectrum. Its frequency is measured to be $\omega = (0.84 \pm 0.1)\omega_{pe}$ and corresponds to the coupling of the runaway branch with the ω_1 branch from Fig. 9(a). The mode with the highest energy in the runaway phase is mode 3, with a measured frequency of $\omega = (0.46 \pm 0.1)\omega_{pe}$. It falls on the runaway branch but appears to be a coupling of the runaway mode ($\omega = kv_f \cos\theta$) and the ω_2 mode [Fig. 9(b)].

We have plotted in Fig. 9(c) the electromagnetic simulation frequency against the theoretical normal mode dispersion relation. Only the runaway branch ($\omega \sim kv_f \cos\theta$) and the whistler, upper-hybrid and light branches appear there. The beam cyclotron resonances do not appear in the electromagnetic component of the spectrum. The runaway branch has the highest spectral intensity, as in the electrostatic component of the spectrum. The spectral intensities in both electrostatic and electromagnetic components of the spectrum are of the

same order of magnitude, in agreement with Fig. 3(a) and Fig. 5(d) where electrostatic and magnetic energies are seen to achieve the same level in the runaway phase. Modes 3 and 6 have the highest spectral intensities of all the runaway modes. The frequency of mode 6 is measured at the same value as in the electrostatic dispersion relation of $\omega = (0.84 \pm 0.1)\omega_{pe}$. It is a result of the coupling between the upper-hybrid (or ω_1) branch with $\omega \sim \omega_{pe}$ and the runaway branch. The frequency of mode 3 is the same as its electrostatic counterpart at $\omega = (0.46 \pm 0.1)\omega_{pe}$. Mode 4 which achieves the highest energy among the magnetic modes in the runaway phase has $\omega = (0.6 \pm 0.1)\omega_{pe}$. This mode also appears in the electrostatic component of the spectrum where it achieved the second highest energy in the runaway phase. Both modes 3 and 4 have low enough frequencies ($\omega \ll \omega_{pe}$) and broad enough spectral peaks to be located on the whistler (or ω_2) branch. The excited waves affect the runaway electrons in turn. In Figs. 10(a) and (b) we see that the radiation is emitted in a very spiky, intermittent fashion in time. This bursty radiation emittance is due to the incessant coming and going of resonance of runaway electrons with radiative modes. The secular increase of runaway electron momenta is reduced from the value of free fall because of the wave-particle interaction. In the previous work (Leboeuf and Tajima, 1979a) when only the electrostatic interaction was retained, the rate of momentum increase in time was $\sim 2/3$ of the free fall (not shown in Fig. 10). When the electromagnetic interaction is included, we find that the increase of momenta is further reduced to $\sim 1/3$ of the free fall value [Fig. 10(c)]. This is because the beam experiences more drag by emitting EM waves. We find that the larger the tilt angle is, the more slowdown of the runaway momenta results. This means that if we had tried two-dimensional simulation allowing various modes with various tilt angles simultaneously, most electron slowing down would happen by waves propagating in directions oblique to the magnetic field.

We see occasionally a complete stopping of the increase of the runaway momenta, which is called the clamping of the runaway momenta. When clamping occurs, it is accompanied by a

large and fast spreading in perpendicular momentum of the distribution function. Contours of the distribution function in (p_x, p_y) space are displayed in Fig. 11(a) (before clamping) and 11(b) (after clamping). Perpendicular spreading is a consequence of energy conservation in the wave frame, i.e., if $p_{||}$ decreases, $p_\perp$ has to increase to conserve energy. This is somewhat difficult to quantify because of the dc electric field. In this case we observe the strong excitation of magnetic modes (corresponding to a magnetic energy increase by a factor 10 over the level without ions) at the fundamental wavelength L_x (mode 1) and the $L_x/2$ one (mode 2) with frequencies on the Alfvén-ion cyclotron branch which accounts for the clamping and reduction of $\overline{p}$.

The excitation of Alfvén ion-cyclotron waves in our electromagnetic simulations is the following. The drifting electrons see the electromagnetic ion-cyclotron wave at their own cyclotron frequency, interact with the wave and give up their energy to it, if the cyclotron resonance condition $\omega - kv_b + \omega_{ce}/\gamma = 0$ is satisfied (Hasegawa, 1975). Here $\omega \simeq \omega_{ci}$, when ω_{ci} is the ion-cyclotron frequency; k and v_b are respectively the wavevector and electron velocity parallel to the magnetic field. It is then the interaction of the beam-cyclotron mode and the Alfvén ion-cyclotron mode which leads to wave growth. To quantify this process, we place ourselves in the limit of zero tilt angle. The dispersion relation for the electron beam-plasma system may be written as

$$\omega^2 - k^2c^2 - \omega_{pe}^2\left(\frac{\omega}{\omega+\omega_{ce}}\right) - \omega_{pi}^2\left(\frac{\omega}{\omega-\omega_{ci}}\right) - \left(\frac{\omega_{pb}^2}{\gamma}\right)\left[\frac{(\omega-kv_b)}{(\omega-kv_b+\omega_{ce}/\gamma)}\right] = 0 \qquad (10)$$

for the electromagnetic part. Here the electromagnetic dispersion decouples from the electrostatic one (Godfrey *et al.*, 1975). In the above ω_{pb} is the beam plasma frequency. An approximate solution of Eq. (10) yields growth at $\omega \simeq \omega_{ci}$ and $k \simeq \omega_{ce}/\gamma v_b$. A numerical solution with the simulation parameters yields $\omega/\omega_{pe} \simeq 0.02$ and $kL_x/2\pi \simeq 1$, for the most rapidly growing mode. The real frequency is on the Alfvén ion-cyclotron branch.

V. APPLICATIONS IN ASTROPHYSICS

Electromagnetic simulations of the beam-plasma instability and evolution after tail formation in the presence of a constant electric field have been performed and analyzed in view of high-frequency electromagnetic radiation. The initial beam is parallel to the electric and magnetic fields. Its final remnant was found similar to a runaway tail, a characteristic of electron momentum distributions in electric currents. In agreement with previous simulations we note that (i) the runaway particles convert the energy of the dc electric field into plasma wave (ac) energy; (ii) there is a runaway branch with frequencies $\omega \lesssim kc\cos\theta$, which strongly couples to the normal modes of the system; (iii) the runaway electrons are dragged by these modes while $E_{\rm dc}$ is being applied. The inclusion of electromagnetic effects shows that (iv) in the later runaway phase the fraction of wave energy in electromagnetic modes increases to over 50% as we have seen in Fig. 3(a); (v) the low-frequency magnetic modes are strongly excited in the phase of clamping of the runaways; (vi) propagating electromagnetic ordinary (and to a lesser extent extraordinary) waves are emitted and can yield intense observable emission. The most intense electromagnetic wave is from $\omega \sim \omega_{pe}$ shown by a triangle in Figs. 8 and 9(a) (more than three quarters of the intensity of the entire electromagnetic radiation, depending on various conditions except for the case of the magnetic mode excitation). Modes with $\omega \gtrsim \omega_{pe}$ can most likely radiate out. The main spectrum $\omega \sim \omega_{pe}$ can be radiative if the wave propagates toward a more tenuous plasma. The wave energy of $\omega > \omega_{pe}$ originally in our simulation is probably less than 10% of the entire electromagnetic wave energy. The mainly magnetic mode such as the Alfvén waves could be mode converted into propagating electromagnetic waves as Steinolfson, *et al.* (1989) have investigated. Similarly, electrostatic waves can be converted into electromagnetic waves by a density gradient (Melrose, 1980) in real plasmas. The efficiency of this direct conversion scales with the inverse density scale length. Small density structures are generally expected in current sheets as well as in MHD waves resulting from reconnection. Electromagnetic waves above the cut-off

frequencies are of particular interest to astrophysics. Our simulations clearly show that their two branches couple to the runaway tail of the electron distribution.

The simulations have been made for strong electric fields far beyond the Dreicer value to reduce computing time. Leboeuf, *et al.* (1979b) have found a decreasing level of wave energy for smaller $E_{\rm dc}$. At $\widetilde{E}_{\rm dc} \approx 0.1$ this decrease, however, is weak enough to suggest a considerable effect also at smaller electric fields above the Dreicer limit. On the other hand, when we increase the acceleration, the level of wave energy and thus the radiation increases rapidly as a function of $E_{\rm dc}$, until it reaches maximum when $E_{\rm dc}$ reaches the value defined by $E_{\rm es}$ in Eq. (5). Beyond this, no beam-instability and thus no radiation is observed. That is, when the acceleration due to $E_{\rm dc}$ is too large, the beam-plasma system fails to sustain the beam-plasma instability. This effect may play an important role in radiation processes for accreting matter near compact massive objects such as a black hole. For example, accreting matter under the influence of gravitation radiates in the ambient magnetized corona ever so brightly until it reaches the level defined by Eq. (5) and ceases its collective radiative process. It is worthy to notice that this acceleration can be reached before matter accretes within the Schwarzschild radius.

Let $W(k)$ be the energy density of propagating transverse waves with wavevector k. Their brightness temperature becomes (using the Rayleigh-Jeans approximation)

$$T_B = \frac{1}{2}\frac{a}{\pi b}\frac{nc^3}{\nu^3}T_0 \ , \tag{11}$$

where T_0 is the ambient electron temperature in energy units and we have used $v_{gr} \approx c$, and put the total wave energy density as

$$\frac{W(k)k^2\Delta k}{8\pi^3}\frac{\Delta r}{4\pi} = anT_0 \tag{12}$$

with a determined by the simulations, the bandwidth defined by $\Delta\nu = b\nu$, and the emission solid angle $\Delta r \approx \pi$. Emission by coupling the runaway (or beam) branches is expected to be

very narrow-banded as we observed in Sec. IVa. We will use $b = 10^{-1} - 10^{-3}$ in the numerical estimates.

Spatially uniform dc fields above the Dreicer limit may be expected in a wide variety of astrophysical plasmas. Here we consider as an example impulsive reconnection suggested for solar and stellar flares. In the general scenario (e.g., Heyvaerts, *et al.*, 1977) the size of the current layer between two regions of differently directed magnetic fields decreases due to external motions. As soon as the current becomes unstable, the resistivity suddenly increases due to coupling between particles and waves leading to explosive annihilation of the magnetic field. Assuming the current constant, The induced impulsive electric field by magnetic field annihilation reaches a value of

$$E_{\rm imp} = E_0 \frac{\eta_{\rm turb}}{\eta_0} \ , \tag{13}$$

where E_0 and η_0 are initial electric field and resistivity, and $\eta_{\rm turb}$ is the anomalous resistivity due to wave turbulence. E_0 is given by $E_0 = (c/v_\infty)\, B$, where v_∞ is the contraction velocity of the reconnection region at infinity. If the turbulent collision frequency $\nu_{\rm turb}$ is determined by the electron dynamics in the direction out of the plane of reconnection, the resistivity may be assessed by studying the wave drag on electrons seen in our simulation. Let the equation of motion along the magnetic field near the reconnection point

$$\dot{p} = eE_{\rm dc} - \nu_{\rm turb}\, p \ , \tag{14}$$

where the dc electric field $E_{\rm dc}$ is produced by the reconnection. From our simulation Fig. 10(c) we learn

$$\dot{p} \cong \frac{1}{3}\, e\, E_{\rm dc} \ . \tag{15}$$

In this case Eqs. (14) and (15) imply

$$\nu_{\rm turb}\, p \cong \frac{2}{3}\, e\, E_{\rm dc} \ . \tag{16}$$

With $E_{\rm dc} = 0.2m\,\omega_p^2\,\Delta/e$ and $p \sim mc$, Eq. (16) leads the evaluation of $\nu_{\rm turb}$ as

$$\nu_{\rm turb} \sim 10^{-2}\,\omega_p\ , \tag{17}$$

and $\eta_{\rm turb} = 4\pi\nu_{\rm turb}/\omega_p^2 = 4\pi 10^{-2}\omega_p^{-1}$.

The impulsive electric field decreases from its value given in Eq. (12) with the spread of the current sheet. It expands with a velocity $c^2\eta_{\rm turb}/4\pi l$, where l is the thickness of the current sheet (Heyvaerts, *et al.*, 1977). The electric field falls back to the value E_0 after a time

$$\Delta t = \frac{\eta_{\rm turb}}{4\pi}\left(\frac{c}{v_\infty}\right)^2\ . \tag{18}$$

Let us use $\omega_p = 2\pi\cdot 3\times 10^9\,{\rm Hz}$, and $v_\infty = 100\,{\rm km/s}$ for coronal conditions. Equation (18) then yields Δt on the order of 10 ms.

The temperature T_0 in the current sheet is of the order of 10^6K and the electron density of this process is believed to be in the range of $10^9 - 10^{12}{\rm cm}^{-3}$. Emissions near the plasma frequency are thus in the range of 0.3–10 GHz. Our simulations are too limited to yield a reliable estimate of the fraction a of transverse wave energy. We will use $a = 10^{-4}$ compatible with $\tilde{E}_{\rm dc} = 0.2$ at $\omega_{pe}t = 400$ (cf. Fig. 3). The brightness temperature, given by Eq. (11), and using the above value for T_0 and ω_p then yields $10^{16} - 10^{18}\,{\rm K}$.

The above example shows a possible scenario of current driven (or acceleration driven) radiation in astrophysics. The present mechanism could provide a physical process for intense spiky radio bursts often observed from solar flares, which have a very bright radiation temperature ($\sim 10^{15}\,{\rm K}$) and bursty in time and narrow in spectral width. Future simulations closer to reality in ion mass, electric field strength, duration, etc., are required for actual models. Nevertheless, the present simulation and discussion have shown the existence of an efficient radiation process, which can be the observable signature of a strong current in astrophysical plasmas. The present instability is primarily due to the beam Landau resonance. However, an equally effective radiative emission due to the beam cyclotron resonance is pos-

sible. (Recall our parameters were such that $\omega_{pe} = \omega_{ce}$ in most runs). This is often called the gyrotron instability (or the cyclotron resonance maser) (for example, Hirshfield and Granatstein, 1977). Further, the cyclotron autoresonance maser instability (Pelenin, 1974) is a similar but distinct radiative mechanism. When the beam is driven by a dc electric field (or gravitational) acceleration, we expect that the driven gyrotron emission would also have an intense, bursty and bright, spectrum around ω_{ce}. However, a detailed investigation of this problem is left for the future.

Acknowledgements

This work was partially supported by the National Science Foundation Grant ATM-88-10539, and the United States Department of Energy Grant DE-FG05-80ET-53088. The work at ETH Zurich was partially supported by the Swiss National Science Foundation (Grant 2-4.919).

References

Bell, T.F., 1965, *Phys. Fluids*, **8**, 1829.

Benz, A.O., 1986, *Solar Phys.*, **104**, 99.

Boris, J.P., Dawson, J.M., Orens, J.H., and Roberts, K.V., 1970, *Phys. Rev. Lett.*, **25**, 706.

Dawson, J.M. and Shanny, R., 1968, *Phys. Fluids*, **11**, 155.

Dreicer, H., 1959, *Physical Review*, **115**, 238.

Godfrey, B.B., Shanahan, W.R., and Thode, L.E., 1975, *Phys. Fluids*, **18**, 346.

Gurnett, D., 1981, in *Formation of Auroral Arcs*, Geophysical Monograph Series, ed. S.I. Akasofu (American Geophysical Union, Washington, D.C.).

Hasegawa, A., 1975, *Plasma Instabilities and Nonlinear Effects* (Springer-Verlag, New York) p. 49.

Heyvaerts, J., Priest, E.R., and Rust, D.M., 1977, *Astrophys. J.*, **216**, 123.

Hirose, A. and Skarsgaard, H.M., 1976, *Phys. Rev. Lett.*, **36**, 252.

Hirshfield, J.L. and Granatstein, V.L., 1977, *IEEE Trans. Micro Theor. Tech.*, **25**, 522.

Holman, G.D., Eichler, D., Kundu, M.R., 1980, *IAU-Symposium Radio Physics of the Sun*, 457-459.

Kainer, S., Dawson, J.M., Shanny, R., and Coffey, T.P., 1972, *Phys. Fluids*, **15**, 493.

Koga, J., Geary, J.L., Fujinami, T., Newberger, B., Tajima, T., and Rostoker, N., 1989, *J. Plasma Phys.*, (to be published).

Kruer, W., 1988, *Laser-Plasma Interaction*, (Addison-Wesley, Redwood City).

Leboeuf, J.N. and Tajima, T., 1979a, *Phys. Fluids*, **22**, 1485.

Leboeuf, J.N. and Tajima, T., 1979b, *Appl. Phys. Lett.*, **34**, 548.

Melrose, D.B., 1980a, *Aust. J. Phys.*, **33**, 121.

Menyuk, C., Hammer, D, and Morales, G.J., 1977, *Bull. Am. Phys. Soc.*, **22**, 1200.

Mikhailovskii, A.B., 1974, *Theory of Plasma Instabilities*, Vol. I, (Consultant Bureau, New York) p. 160.

Nishikawa, K. 1968, *J. Phys. Soc. Jpn.*, **24**, 1152.

Oomens, A.A., Ornstein, L.Th.M., Parker, R.R., Schuller, F.C., and Taylor, R.J., 1976, *Phys. Rev. Lett.*, **36**, 255.

Parail, V.V. and Pogutse, O.P., 1976, *Sov. J. Plasma Phys.*, **2**, 125.

Pelenin, M.I., 1974, *Radiophys. Quant. Elect.*, **17**, 686. Sagdeev, R.Z. and Galeev, A.A., 1969, *Nonlinear Plasma Theory*, (Benjamin, New York).

Schmidt, G., 1960, *Phys. Fluids*, **3**, 961.

Steinolfson, R.S., Pereira, V., Mahajan, S.M., and Tajima, T., 1989, to be published.

Tajima, T., 1989, *Computational Plasma Physics with Applications to Fusion and Astrophysics*, (Addison-Wesley, Redwood City).

Tajima, T., 1984, *Laser Part. Beams*, **3**, 351.

Tammaru, I., Electron Dynamics Laboratories, Hughes Aircraft Co., Private Communication.

Thode, L.E. and Sudan, R.N., 1973, *Phys. Rev. Lett.*, **30**, 732.

Wagner, J.S., Tajima, T., Kan, J.R., Leboeuf, J.N., Akasofu, S.I., and Dawson, J.M., 1980, *Phys. Rev. Lett.*, **45**, 803.

Wagner, J.S., Lee, L.C., Wu, C.S., and Tajima, T., 1983, *Geophys. Res. Lett.*, **10(6)**, 483.

Wu, C.S. and Lee, L.C., 1979, *Astrophys. J.*, **230**, 621.

Wu, C.S., Zhou, G.C., and Gaffey, J.D., Jr., 1985, *Phys. Fluids*, **28(3)**, 846.

Figure Captions

1. This diagram defines the tilt angle θ and the beam propagation and guide magnetic field directions along which the dc electric field is applied.

2. The electromagnetic magnetized beam-plasma instability without dc field and at various tilt angles θ.
   (a) Maximum growth rate versus tilt angle θ for the electrostatic field (dots) and the magnetic field (triangles). The circles represent theory. The solid line is a fit to $\cos^2\theta$.
   (b) Most energetic mode number versus θ for the electrostatic field (circles) and magnetic fields (triangles).
   (c) Saturation time versus tilt angle θ for the electrostatic energy (dots) and magnetic energy (triangles).
   (d) Saturation energy versus θ for the electrostatic (circles), transverse electric (dots) and magnetic (triangles) fields.

3. Time evolution of the field energies at $\theta = 15°$ for (a) $\tilde{E}_{\rm dc} = 0.2$ and (b) $E_{\rm dc} = 0$. The solid curves represent the magnetic energy, the dashed ones the transverse electric energy, and the dash-dot ones the electrostatic energy.

4. Schematic drawing of the phase space trajectories for electrons moving in a potential wave and acted upon by the dc electric field.

5. The electromagnetic magnetized beam-plasma instability with dc field and various tilt angles θ.
   (a) Electrostatic energy in the beam-plasma phase for $E_{\rm dc} = 0$ (circles), $\tilde{E}_{\rm dc} = 0.2$ (dots) and in the runaway phase (triangles).
   (b) Magnetic energy and (c) transverse electric energy in the same phases.
   (d) Maximum energy achieved in the same unit. If electrostatic, a circle is plotted; if magnetic, a triangle is drawn.

6. Dispersion relation for $\theta = 15°$ and $E_{\rm dc} = 0$. The simulated frequencies are indicated by dots, theory by solid lines. The modes with highest spectral intensity are represented by triangles.
   (a) Electrostatic component plotted against the normal modes of the system.

(b) Electrostatic component plotted against the beam dispersion relation with $p_b = 7.63mv_{te}$ and $n_b = 0.1n_p$.
(c) Electromagnetic component plotted against the normal modes. The theoretical beam branch is drawn in as a dashed line in (a) and (c).

7. Dispersion relation for $\theta = 45°$ and $E_{\rm dc} = 0$. (a) Electrostatic component versus the normal modes. (b) Electrostatic component versus the beam-plasma dispersion relation. (c) Electromagnetic component versus the normall modes. The theoretical beam branch is drawn in as a dashed line in (a) and (c).

8. Electrostatic dispersion relation for $\theta = 0°$ and $\widetilde{E}_{\rm dc} = 0.2$. The simulation frequencies are represented by dots. The modes with highest spectral intensity are indicated by triangles. The theoretical beam dispersion relation with $\langle p \rangle = 7mc$ and $\langle n \rangle = 0.2n_p$ is drawn in as full lines. The dashed line represents the $2\omega_{pe}$ harmonic.

9. Dispersion relations for $\theta = 45°$ and $\widetilde{E}_{\rm dc} = 0.2$.
(a) Electrostatic component versus the normal modes.
(b) Electrostatic component versus the beam-plasma dispersion relation with $\langle p \rangle = 20mc$ and $\langle n \rangle = 0.25n_p$.
(c) Electromagnetic component versus the normal modes. The theoretical runaway branch (a,c) and Doppler-shifted cyclotron modes are drawn as dashed line (a).

10. Time evolution of the energy of the runaway mode 5 for $\theta = 15°$ and $\widetilde{E}_{\rm dc} = 0.2$ in (a) the z component of the magnetic field, (b) the y component of the electric field as compared to (c) the evolution of the runaway momentum where the full line denotes free fall and the dashed line the $\frac{2}{3}E_{\rm dc}t$ asymptote. The dash-dot line represents the $\frac{1}{3}E_{\rm dc}t$ asymptote. The dots are the simulation values.

11. A computer illustration of the perpendicular spreading of the momentum distribution function at clamping for $\theta = 45°$: contours of the distribution function in (p_x, p_y) space (a) just before clamping and (b) just after clamping.

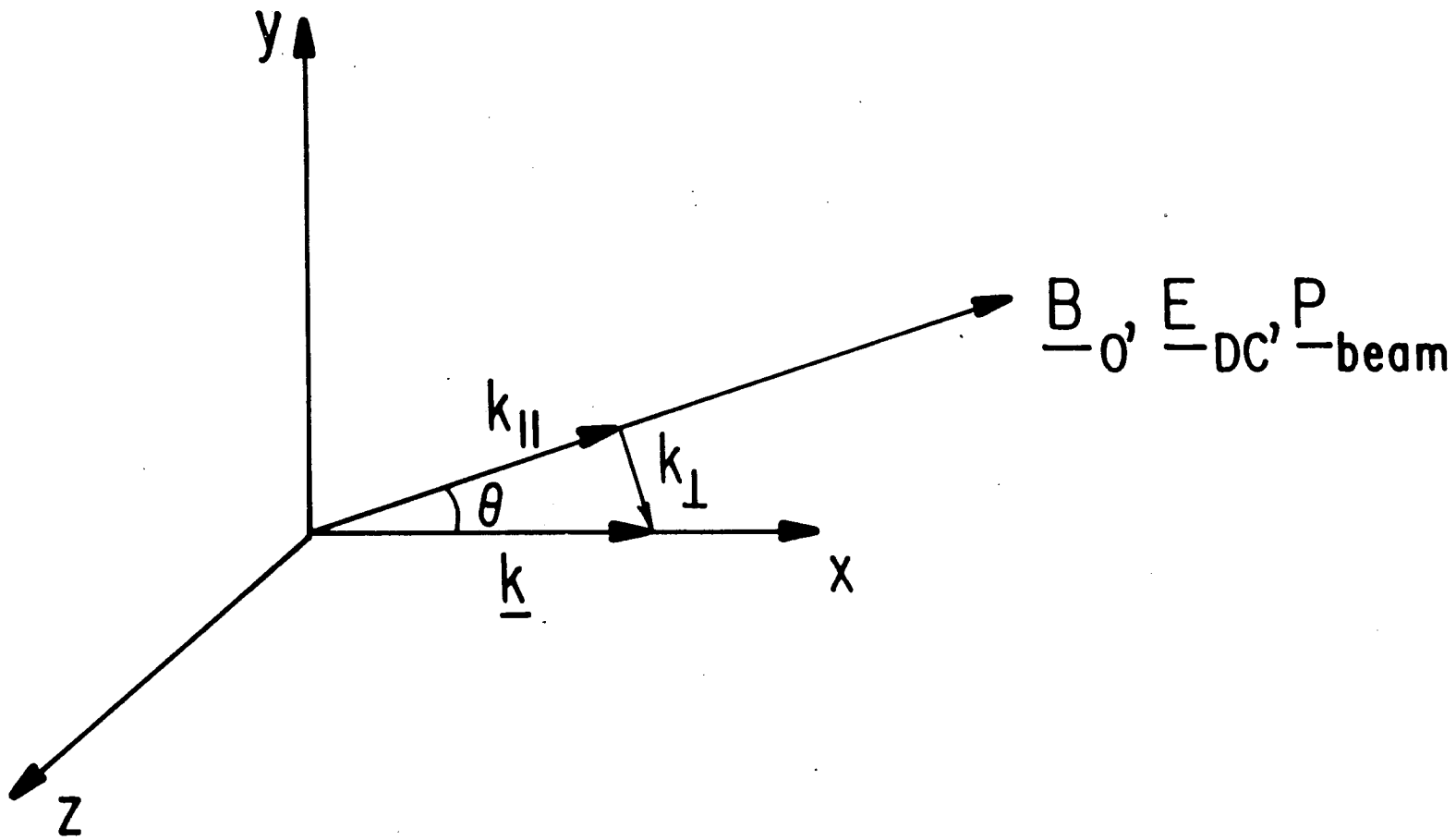
y
$\underline{B}_0, \underline{E}_{DC}, \underline{P}_{beam}$
$k_{\parallel}$
$k_{\perp}$
θ
$\underline{k}$
x
z

Fig. 1

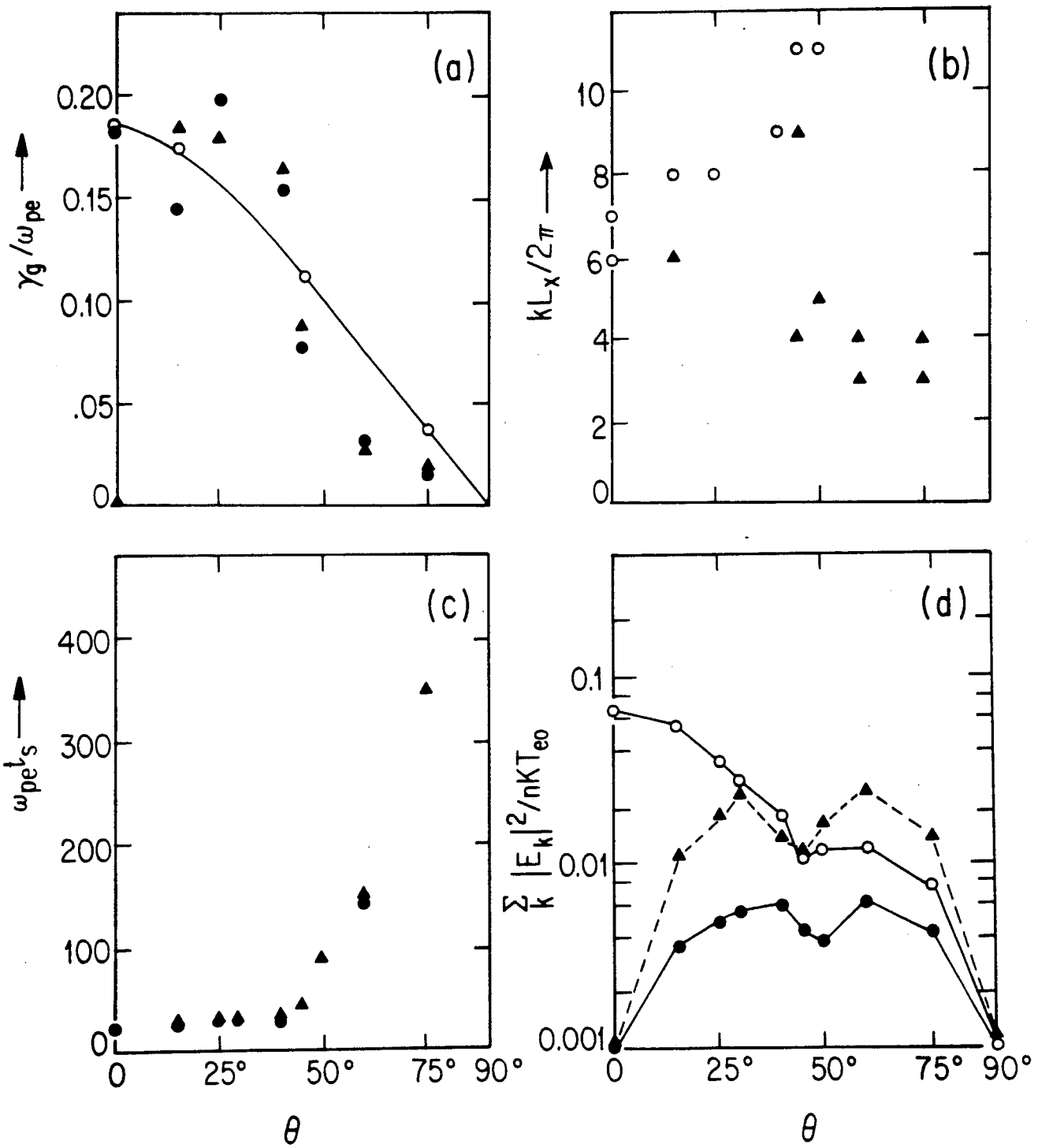
(a)
0.20
0.15
0.10
.05
0
γ_g/ω_{pe}
(b)
10
8
6
4
2
0
$kL_x/2\pi$
(c)
400
300
200
100
0
$\omega_{pe}t_s$
0
25°
50°
75°
90°
θ
(d)
0.1
0.01
0.001
$\Sigma_k |E_k|^2/nKT_{eo}$
0
25°
50°
75°
90°
θ

Fig. 2

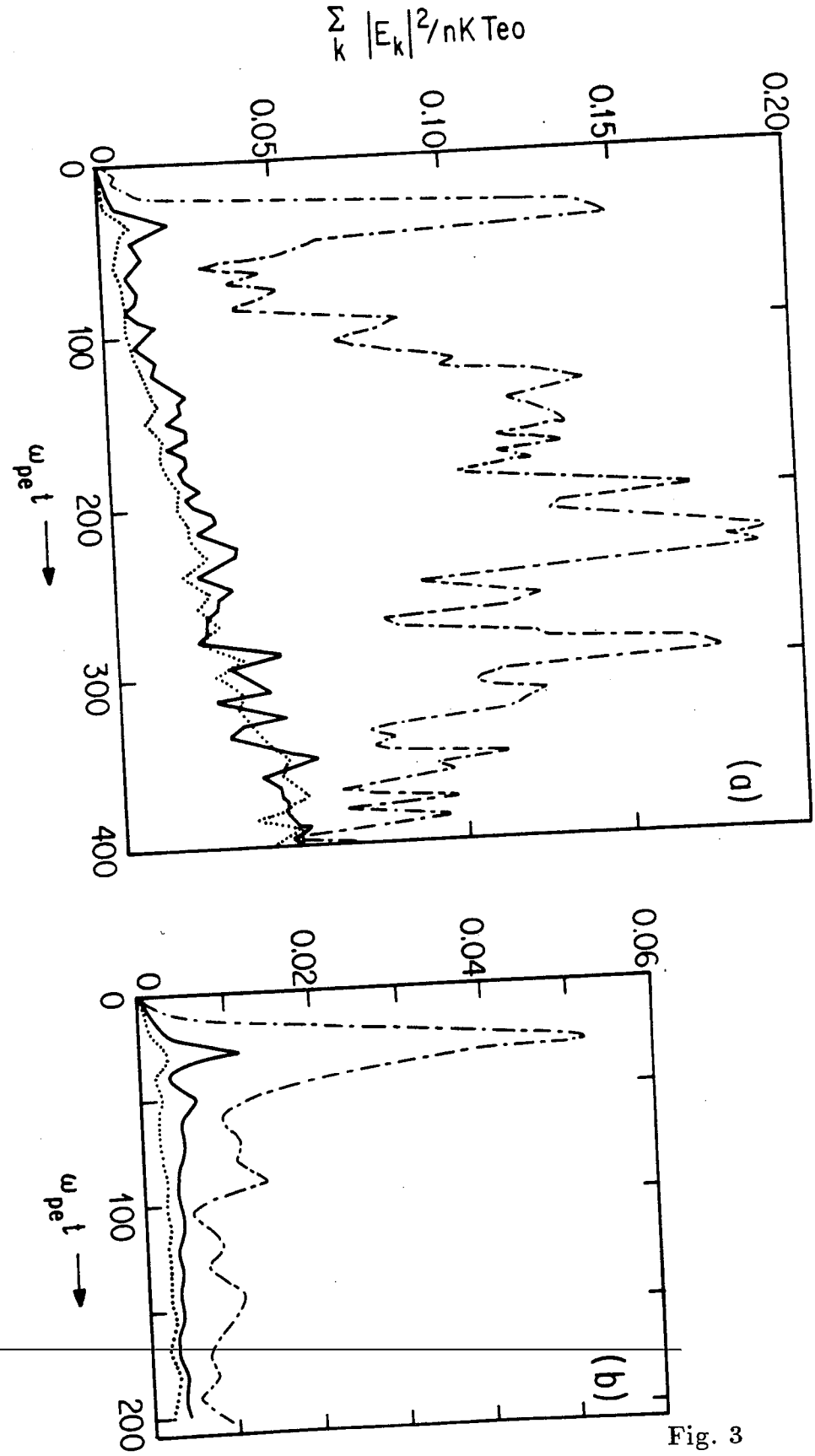
$\sum_k |E_k|^2/nKTeo$
0.05
0.10
0.15
0.20
0
100
200
300
400
$\omega_{pe}t$
(a)
0.02
0.04
0.06
0
100
200
$\omega_{pe}t$
(b)

Fig. 3

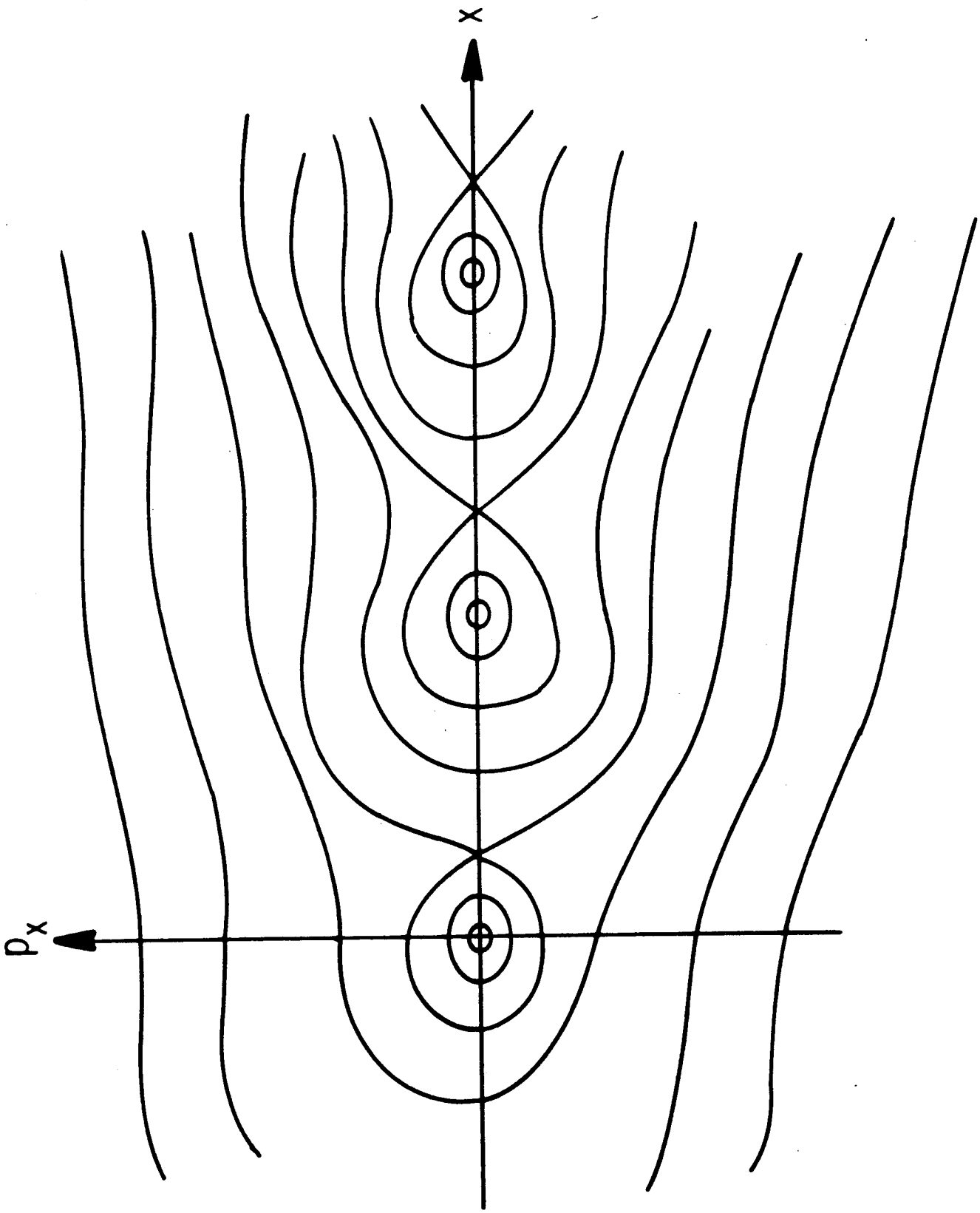

Fig. 4

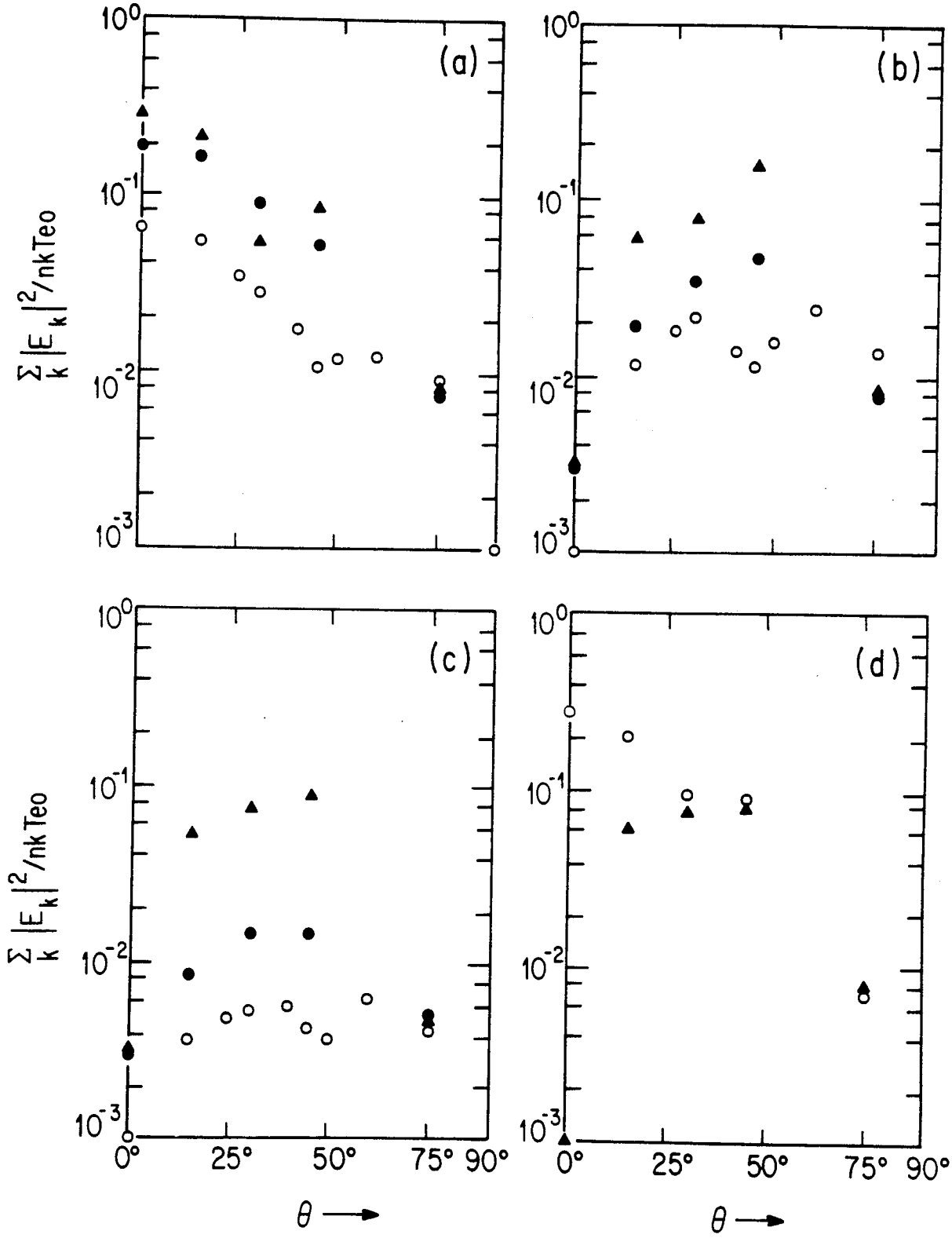

Fig. 5

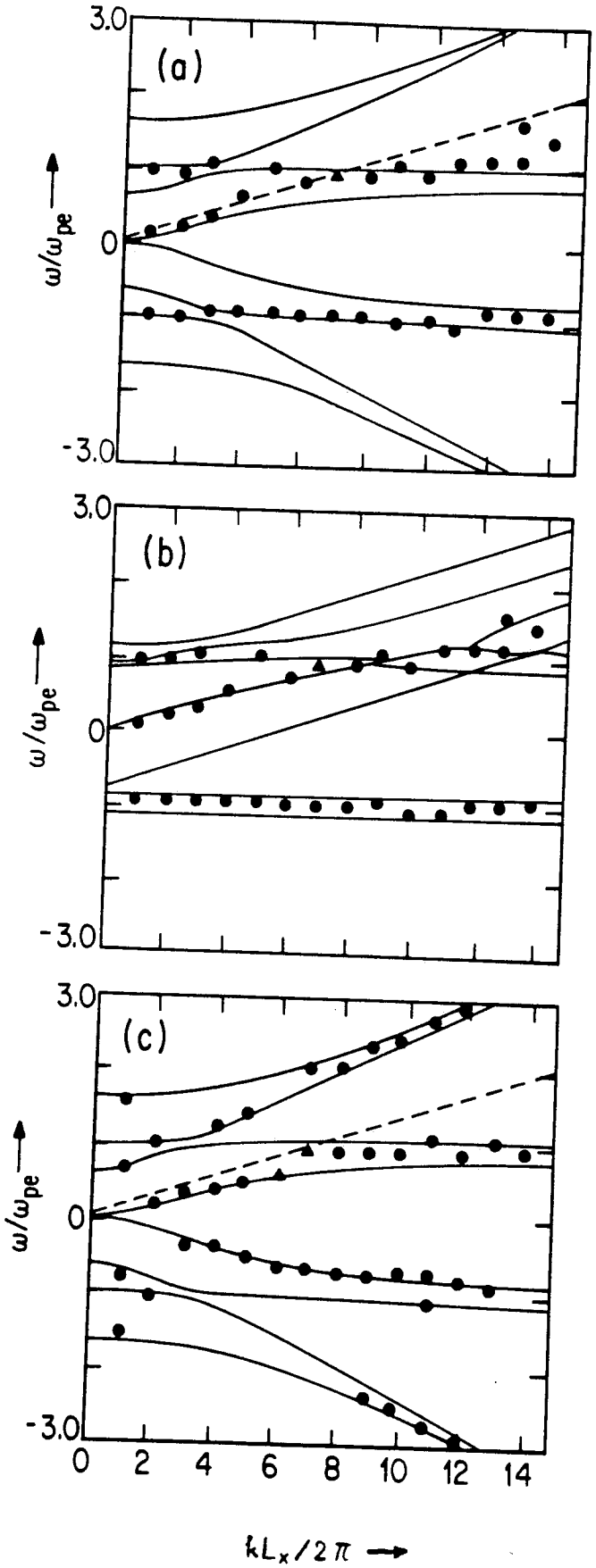

Fig. 6

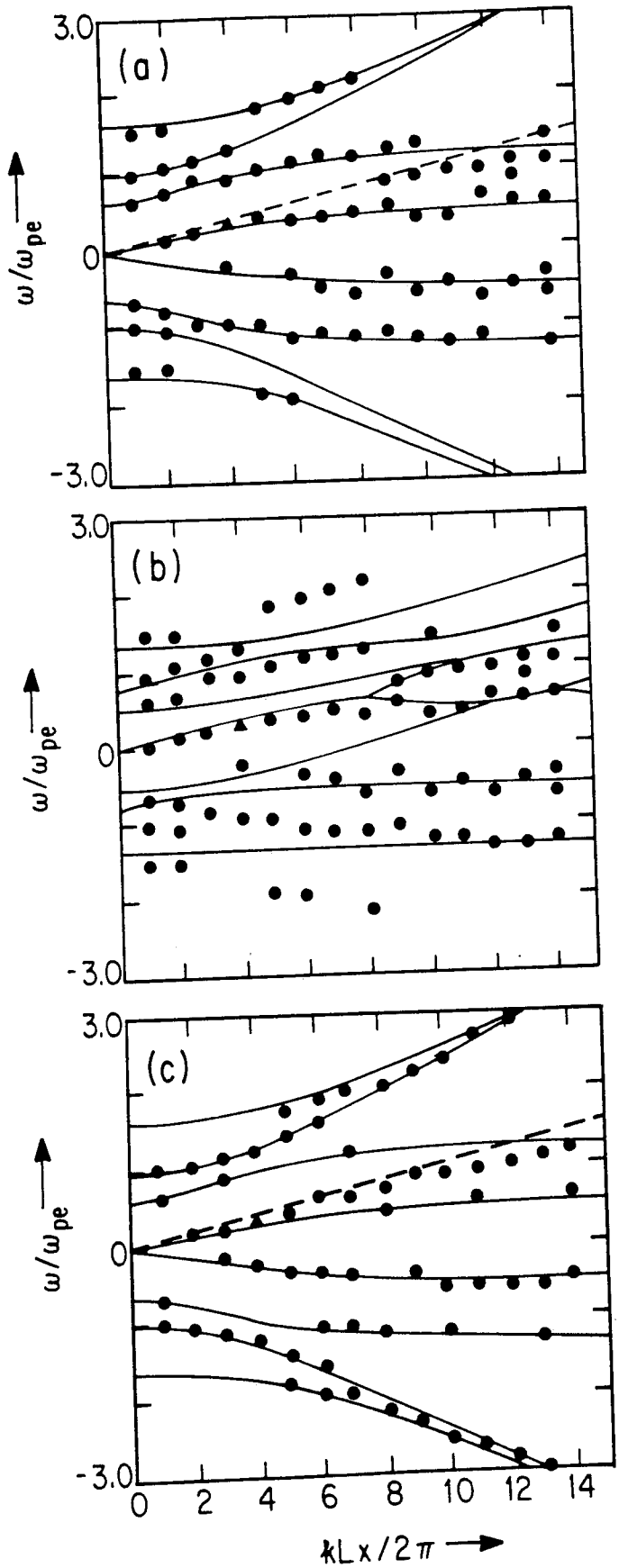

Fig. 7

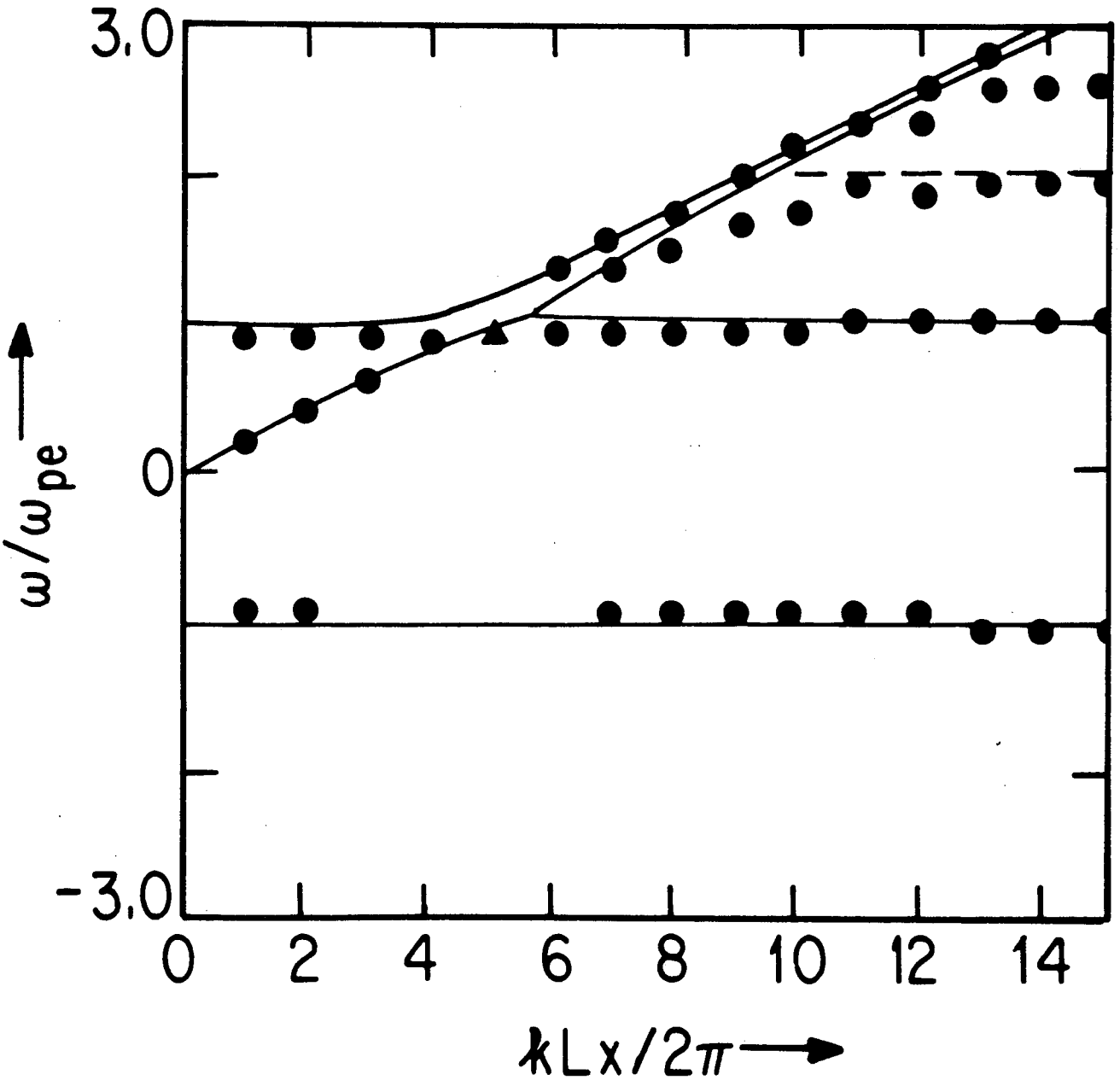

Fig. 8

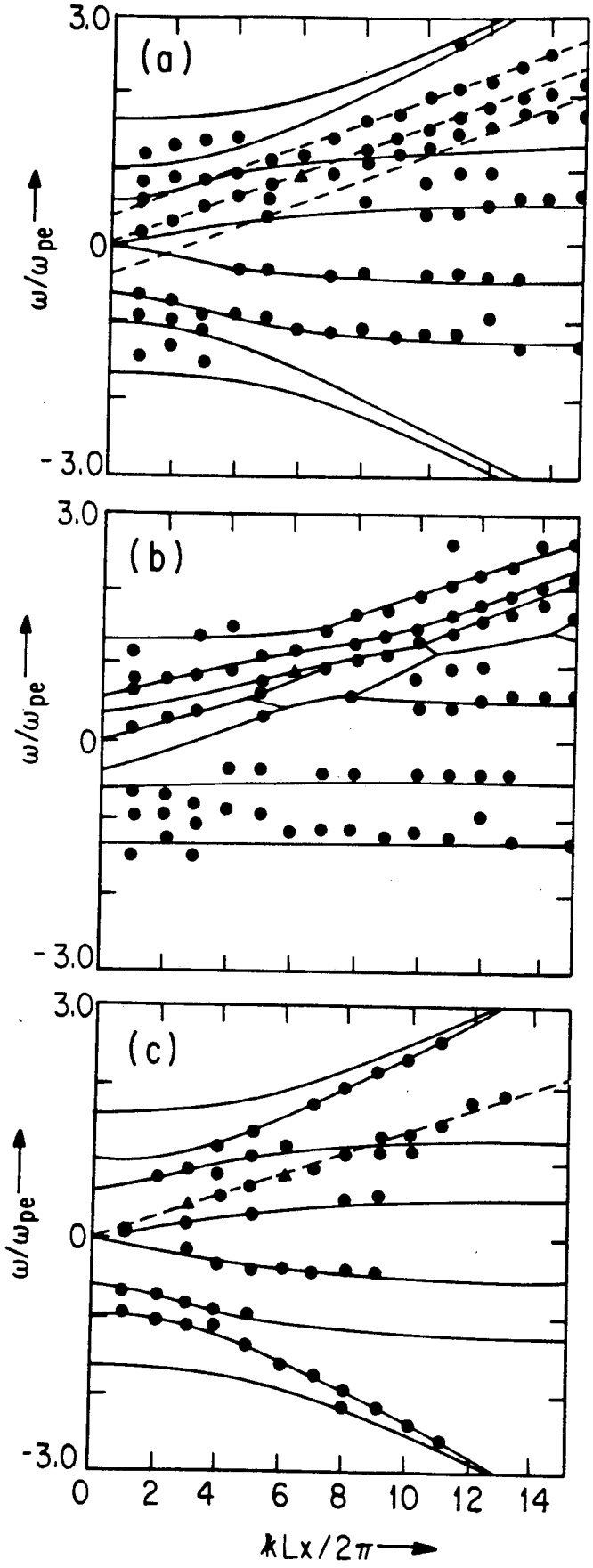

Fig. 9

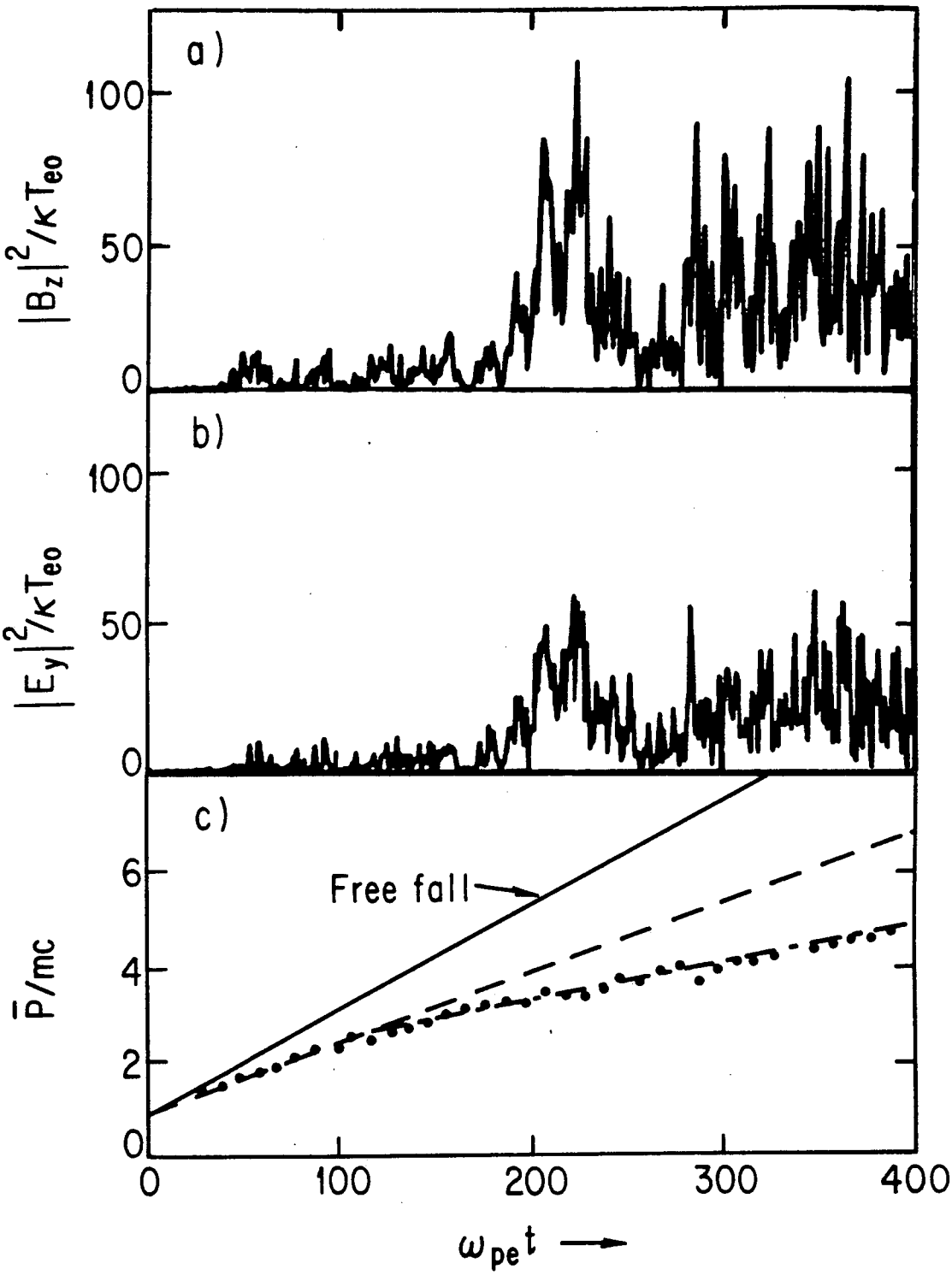
a)
b)
c)
100
50
0
$|B_z|^2/\kappa T_{eo}$
$|E_y|^2/\kappa T_{eo}$
$\bar{P}/mc$
Free fall
6
4
2
0
100
200
300
400
$\omega_{pe}t$

Fig. 10

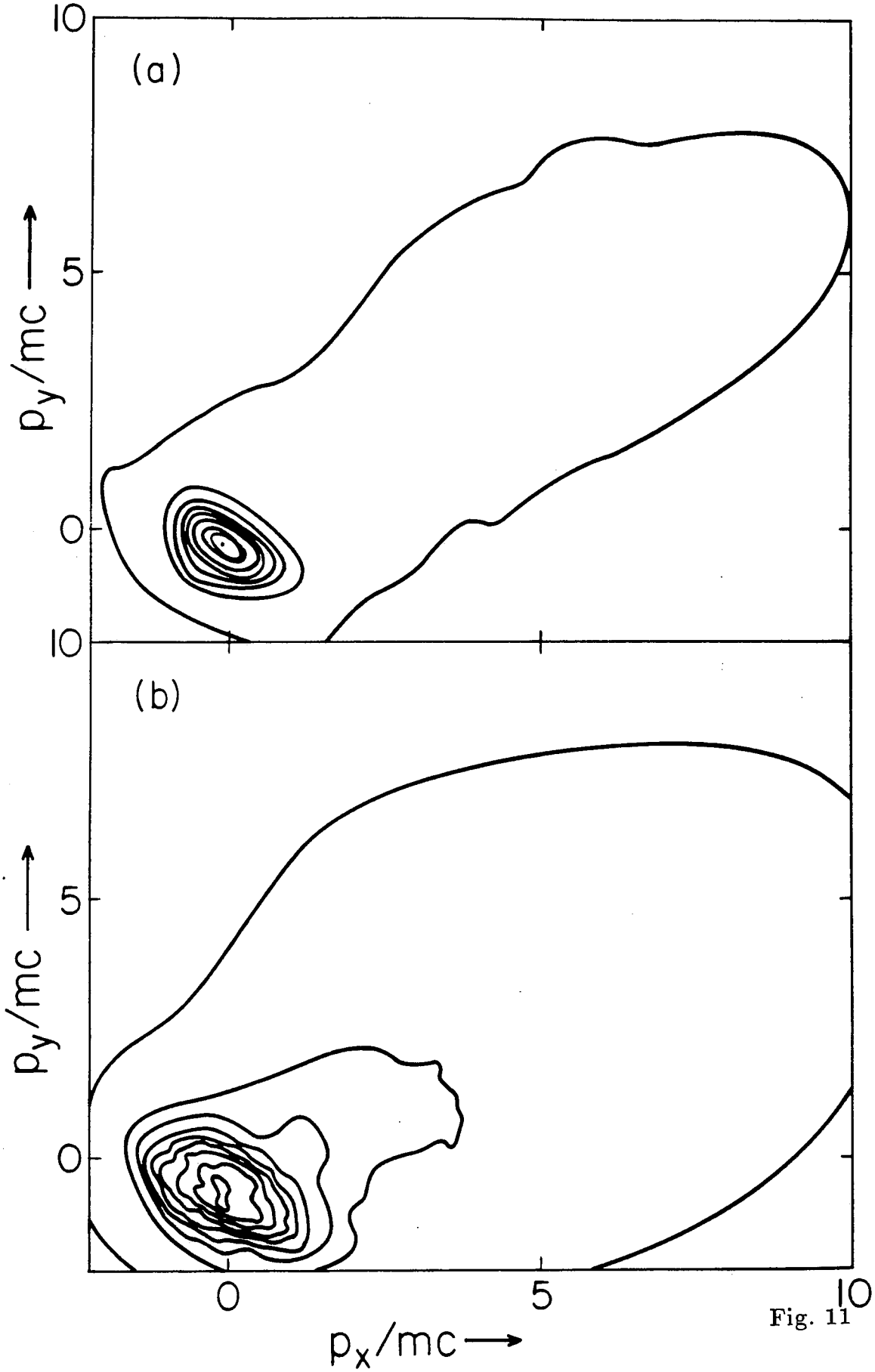

Fig. 11